APPLIED PHYSICS

Pigment darkening as case study of In-Air Plasma-Induced Luminescence

M. Barberio[1,2], E. Skantzakis[3], S. Sorieul[4], P. Antici[1]*

We introduce the use of an In-Air Plasma-Induced Luminescence (In-Air-PIL) spectroscopy as an alternative to classical chemical and crystallographic methods used in materials science. The In-Air-PIL is evaluated on a case study investigating the effect of light aging on the darkening of five pristine yellow pigments commonly used in artworks. We show that the darkening is not associated to changes in the chemical composition, but to a loss in crystallinity, indicating an amorphization process of the pigments induced and catalyzed by the light irradiation. This favors the interaction of the pigment molecules with oxygen and carbon adsorbed from the environment or solved in the binding agent, subsequently leading to the formation of oxalates and carbonates as observed in other works. We demonstrate that the In-Air-PIL results are in perfect agreement with more complex classical materials science analysis methods, making our plasma-driven method a potentially easier and faster technique.

INTRODUCTION

Obtaining exact information about the chemical composition, morphology, and crystal habit of different materials is of major importance in materials science. Classical methods unveiling morphological information include scanning electron microscope (SEM) and atomic force microscope (*1*), whereas chemical information about the materials is obtained by different techniques such as x-ray absorption near-edge structure (*2*, *3*), time-of-flight secondary ion mass spectrometry (*4*, *5*), Raman, x-ray photoelectron spectroscopy, x-ray fluorescence (XRF), and energy-dispersive x-ray (EDX) spectroscopy in SEM. A more sophisticated and costly method for a comprehensive chemical analysis of bulk material is the use of nuclear physics techniques such as particle-induced x-ray emission (PIXE) and particle-induced gamma emission (PIGE) techniques, either driven by a conventional (*6*) or laser-based accelerator (*7*). Recently, we introduced an alternative method suitable to assess the chemical composition, crystal habit, and optical properties of materials using In-Air Plasma-Induced Luminescence (In-Air-PIL) (*8*). We demonstrated in a proof-of-principle experiment that the information acquired with our method was identical to that obtained with the more sophisticated techniques mentioned above (excluding the PIXE and PIGE techniques). Our In-Air-PIL was achieved by the interaction of a focused high-energy laser with air, an interaction that produces a submillimetric plasma. The energetic electrons generated in the plasma and accelerated to energies higher than 5 keV (in our case) reached the sample surface under investigation, causing luminescence emission and plasmonic resonance. This enabled the characterization of various chemical and optical properties. Hence, our In-Air-PIL method allowed for the exact analysis of the sample in terms of chemical composition and crystal habit, covering surfaces in the range of tens of squared millimeter and in the time span of only a few minutes (*8*). In this previous work, we focused solely on the method itself, i.e., how the In-Air-PIL results compared to the classical luminescence techniques. This was carried out to better understand the relevant components that induce the luminescence.

Here, we investigate a possible application of the In-Air-PIL in materials science, choosing the field of cultural heritage, and demonstrate that the technique offers a straight-forward approach to support several more complex spectroscopic methods (e.g., PIXE). This was achieved by using the In-Air-PIL to investigate the darkening process of pictorial pigment layers. Our In-Air-PIL also further provides information about the underlying causes in the darkening effect provoked by light aging, which may explain some observations found in other studies [e.g., (*9*)].

The topic of pictorial pigment layer aging is a very active field of investigation since great demand has been expressed by museums, restorers, and scientists in understanding the causes of color darkening (*10*). This is based on the fact that darkening often results in serious and irreversible damage to precious artwork. Consequently, further insight into the process of pigment darkening is required to better define the conservation and exhibition protocols for paints and objects decorated with pictorial pigment layers. These layers typically consist of inorganic pigments mixed with binding agents, which can be organic or inorganic in frescos, and applied onto a canvas surface. Currently, the main factors that influence the deterioration of pigments are light exposure, humidity, pollution, and microbial contamination (*11*). This can result in different effects such as the formation of a black oxide on the material surface (*12*), the transition of secondary crystalline phases with distinct crystallographic properties (*13*), the absorption of gases from the atmosphere (CO_2, N_2, and O_2), or the formation of a thin biological film on the surface (*14*). The darkening process can also be related to the binding agents and to the structural modification of the supporting materials, i.e., the canvas, wood panel, ceramic, porcelain, etc. (*15*). Typical binding agents used by artists are egg tempera, linseed oil, water, or Arabic gum (*16*). In this scenario, it is thus imperative to understand fully the factors that contribute to the aging of the most important pigments and the subsequent causes of deterioration and darkening. Among environmental risks, light remains one of the most unique since it can never be eliminated nor completely controlled. Light is necessary for viewing the artwork but, since it involves the transmission of energy, can also damage it (*17*).

The darkening of some specific yellow pigments has already been studied. A representative case is chrome yellow, a pigment that is mainly composed of lead chromate and sulfide and that has been extensively used by van Gogh (*18* ,*19*). For instance, at the base of his

[1]Institut National de la Recherche Scientifique (INRS), EMT Research Center, 1650 Boul. Lionel-Boulet, Varennes, QC, J3X 1S2, Canada. [2]Università della Calabria, Dip. DIBEST, Via Bucci 33c, 87036 Rende, Italy. [3]Foundation for Research and Technology-Hellas, Institute of Electronics Structure and Laser, PO Box 1527, GR-71110 Heraklion, Crete, Greece. [4]CENBG, Université de Bordeaux, CNRS/IN2P3, 19 Chemin du Solarium, CS 10-120, 33175 Gradignan, France.
*Corresponding author. Email: patrizio.antici@polytechnique.edu

famous painting "*Les Aliscampes*," large yellow areas have completely lost their brightness, thus becoming dark. The reasons for the yellow deterioration in the van Gogh artwork have been attributed to the formation of a Cr(III)-species and to the loss of orthorhombic crystallinity (*20*). Additional studies have been undertaken in the works of Matisse (*9*), where the authors found that cadmium yellow (CdS) degradation was attributed to the formation of cadmium carbonates and sulphates present in the altered paint layers (*9*). Through the use of a set of spectroscopic and morphologic analysis tools, the authors demonstrated that the deterioration of the yellow, observed in several parts of the painting, was caused by photooxidation products. This effect could also be provoked by residual starting reagents generated from an indirect wet process synthesis of cadmium yellow (*9*).

Currently, little is still known about the darkening mechanisms due to light aging of other yellow pigments that are widely used in paintings by artists ranging from the Babylonian era up to the 19th century. These include the following: Naples yellow ($O_7Pb_2Sb_2$), cadmium yellow (CdS), chrome yellow ($PbCrO_4$), litharge (PbO), and orpiment (As_2O_3). Many of the investigated yellow pigments had their artistic peak in the paintings of the 16th to 19th century. In the paintings "*Sansone e Dalila*" by Rubens (1609) (*21*), "*Ritratto di gentiluomo*" by Tiziano (1510) (*22*), and "*La chambre à Arles*" by van Gogh (1888) (*23*), different pigments were preferred by the individual artists. For instance, Naples yellow was mainly used by "The Old Masters" painters of skill who worked in Europe before 1800 (see as an example "*The Sleeping Venus*" by Giorgione).

Since the role of the main organic binding agent in the darkening process is well known and has already been extensively studied in other works (*19*, *20*), we set our focus on the role of the linseed oil related to the above mentioned five yellow pigments. We also emphasize that the difference between our study and most other papers in the literature that deal with the darkening of pictorial layers is that we concentrate only on the effect of the sunlight irradiation on the pure and pristine pigments without considering the influences of the exposure to environmental agents [as the wet process observed in (*9*)]. Most other authors have analyzed the pigment degradation directly on the original paintings and its effect produced over years, even hundreds of years, by the exposure to light and environmental agents. We focus our attention merely on the effect of sunlight since it is one of the principal causes of the degradation.

RESULTS AND DISCUSSION

We performed our experiments on five pictorial layers composed of two components: an inorganic pigment powder with linseed oil as the binding agent. Details regarding the pigments and their preparation are provided in the Materials and Methods section. We used the five yellow pigments mentioned above (i.e., Naples yellow, cadmium yellow, chrome yellow, litharge, and orpiment) in combination with the linseed oil–binding agent since it is the most commonly used. Moreover, linseed oil has the advantage that its effects on the aging of pictorial layers are well known and can be considered negligible in our case. In addition, many reports including the important studies on chrome yellow (*18*, *19*, *20*) indicate that the degradation of the pictorial layer is independent of the binding agents. This paper is organized as follows: First, we performed optical absorption measurements to test changes in absorption during the aging process (details regarding the experimental setup and measurements can be found in the Materials and Methods section). We also verified the effect of the absorption on the pictorial layers using chemical and morphological analyses. We subsequently applied the In-Air-PIL technique to the different samples and compared the results obtained to other more conventional techniques. Last, we evaluated changes in the crystallinity of the pigments and compared the outcomes with those obtained from the PIXE and luminescence techniques.

The results of the optical absorption measurements are summarized in Fig. 1 and Table 1 for all pigments. It is clear that the absorbance, for all analyzed pictorial layers, increases with aging time in the entire visible range (Fig. 1A), reaching a saturation value that is strictly dependent on the pigment type. The aging causes a decrease in the reflectivity for all spectra in the visible range with a stronger effect at wavelengths approximately 600 nm (yellow) (see Fig. 1A). All the pictorial layers reach a total absorbance (calculated as the normalized integral of the absorbance in the considered spectrum) between 0.8 and 1 (see Fig. 1B). The variation with respect to the nonaged layers varies from 8% for orpiment to 55% for Naples yellow (Table 1). The time to reach saturation, as estimated from the curves in Fig. 1C, varies between 20 and 150 min. (Table 1), indicating a fast aging process for pigments with a low variation in absorbance (chrome yellow and orpiment) and a slow process for the pigments with a very high level of variation (Naples yellow, cadmium yellow, and litharge). No changes were observed in the absorption of pure linseed oil during the 6-hour aging process.

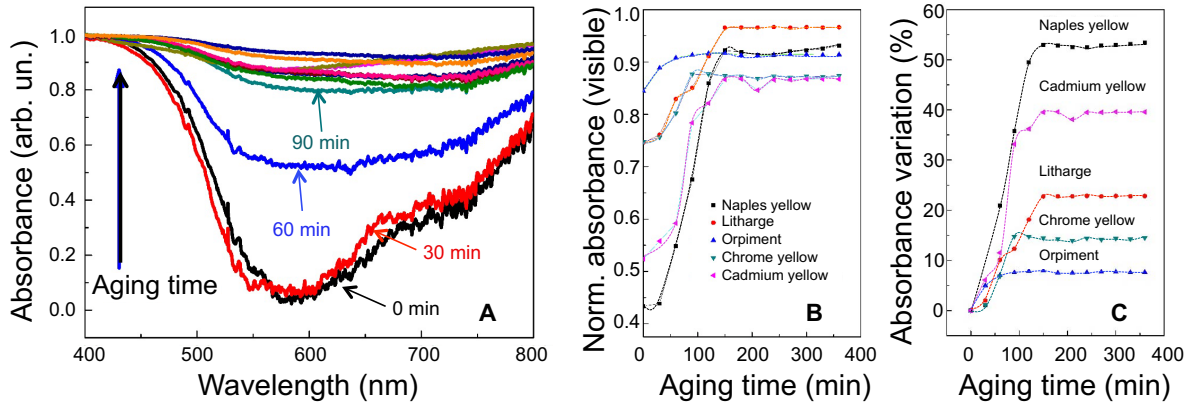

Fig. 1. Optical absorbance. (**A**) Absorbance spectra for Naples yellow taken at regular intervals of 30 min. (**B**) Total absorbance *a* in the entire visible range, obtained as integral of $a(\lambda)$, evaluated between 400 and 800 nm. (**C**) Variation of the total absorbance with respect to the nonaged layers as function of aging time.

Subsequently, we performed chemical analysis of all samples using EDX spectroscopy before and after aging for all the pigment types (see details in the Materials and Method section, the Supplementary Materials, and Table 2). For all the pictorial layers, EDX spectra indicate the presence of the main chemical components that are characteristic for pigments and canvas, i.e., Pb, Sb, S, Cd, Cr, and O, with a small amount of Zn and Ba impurities that are present in the Naples yellow and cadmium yellow pigments (the pigments that show greater changes in absorption). The presence of carbon observed in all pigments was attributed to carbon absorbed from the atmosphere (present in all the materials exposed to atmospheric conditions) by the linseed oil and canvas. Evaluated with the standard oxide method, the chemical composition in all samples (in percent) remains unaffected by aging. Minor variations below 5% are within the limit of experimental error and negligible for this discussion (see the Supplementary Materials). The chemical results undoubtedly indicate the absence of chemical changes during the aging [within the detection limit of our EDX: 1000 parts per million (ppm)], suggesting that the darkening process of the pigments is unrelated to chemical changes, oxide formation, or adsorption-desorption of elements and impurities during aging. The conclusion that the chemical composition does not change is supported by the chemical and morphological analysis of the surface. SEM images of all pigments, obtained before and after aging, indicate that the structure of the pictorial layer surface remains unchanged during the aging process since no macroscopic changes (cracks and fractures) are visible (see the Supplementary Materials).

Having assessed the absorption of the different pigments and the chemical changes during the aging process, we proceeded to irradiate the samples with our In-Air-PIL technique (for details about the experimental setup and the method, see the Supplementary Materials). The plasma used for the In-Air-PIL was generated by the interaction of a focused high-energy laser with air. The laser was operating at a wavelength of 800 nm at a 10-Hz rate delivering pulses of 4 mJ in a duration of 20 fs. The plasma produced in this interaction illuminated our samples over a surface of about 3 cm^2. The In-Air-PIL results are displayed in Fig. 2. The spectra maintained the same structure before and after light irradiation. In particular, we observed four bands for Naples yellow (654, 707, 714, and 762 nm), five bands for orpiment (654, 720, 756, 765, and 773 nm), three bands for chrome yellow (641, 703, and 760 nm), and three bands for cadmium yellow (661, 729, and 768 nm); for litharge, we found bands at 656, 722, and 776 nm. The luminescence band positions, obtained by a Gaussian fit of the original spectra, indicate that the chemical composition of each pigment is unchanged before and after irradiation (see the insets of the different subpanels and the table in Fig. 2). With the exception of one band in the litharge sample (approximately 722 nm), no band shift was observed due to the irradiation, confirming the results of the EDX and PIXE chemical analyses (see below). The band shift before and after irradiation for the second peak of litharge (approximately 722 nm) can be caused by some evaporation of oxygen (as observed also in the PIXE analysis), which causes oxygen vacancies in the lattice structure, resulting in changes in the luminescence emission. In all pigments, all observed bands are comparable with the data available in the classical cathodoluminescence database [CSIRO (*24*) and see also (*25*)] and can be attributed to the intrinsic defects of the crystal lattices (i.e., oxygen and lattice vacancies or extrinsic impurities). For example, the peaks in the orange-red wavelength range (570 to 630 nm) are characteristic of lead oxide composites (orpiment basis) and are usually attributed to oxygen interstitials in PbO (*24*, *25*, *26*), while the band approximately 760 nm in chrome yellow is usually attributed to the CrO_4 emitter (*24*). In all pigments, the strong intensity decrease observed for all bands after the aging process indicates a strong changes in the lattice structure, as confirmed by x-ray diffraction (XRD) analysis (see below). Nevertheless, the In-Air-PIL spectra indicate a strong change in the width of the bands after aging. The red bands located about 650 and 720 nm increase in width by approximately 35% after irradiation. The broadening of the luminescence lines indicate a relaxation in the structural lattice (*25*), which translates from an ordered to a disordered phase. This is in agreement with our crystallographic measurements.

The results obtained on the chemical composition of the surface using both EDX and In-Air-PIL are confirmed by the PIXE analysis

Table 1. Summary of changes in the total absorbance as function of aging time.

Pigments	Increase in absorbance when at saturation value (%)	Aging time for saturation (min)
Naples yellow	55%	150
Cadmium yellow	40%	150
Litharge	25%	150
Chromium yellow	15%	20
Orpiment	8%	20

Table 2. Summary of the EDX results for major constituents (in %).

Naples yellow			Cadmium yellow			Litharge			Chrome yellow			Orpiment		
$O_7Pb_2Sb_2$			CdS			PbO			$PbCrO_4$			As_2S_3		
	Before	After		Before	After		Before	After		Before	After		Before	After
PbO_2	62.70	63.19	SO_3	37.04	37.38	PbO_2	20.88	22.20	PbO_2	80.96	78.81	As_2O_3	50.78	51.16
Sb_2O_3	33.58	33.16	CdO	45.23	44.68	CO_2	79.12	77.80	Cr_2O_3	19.04	21.19	SO_3	49.22	48.84
ZnO	3.72	3.65	BaO	7.23	7.25									
			ZnO	10.50	10.69									

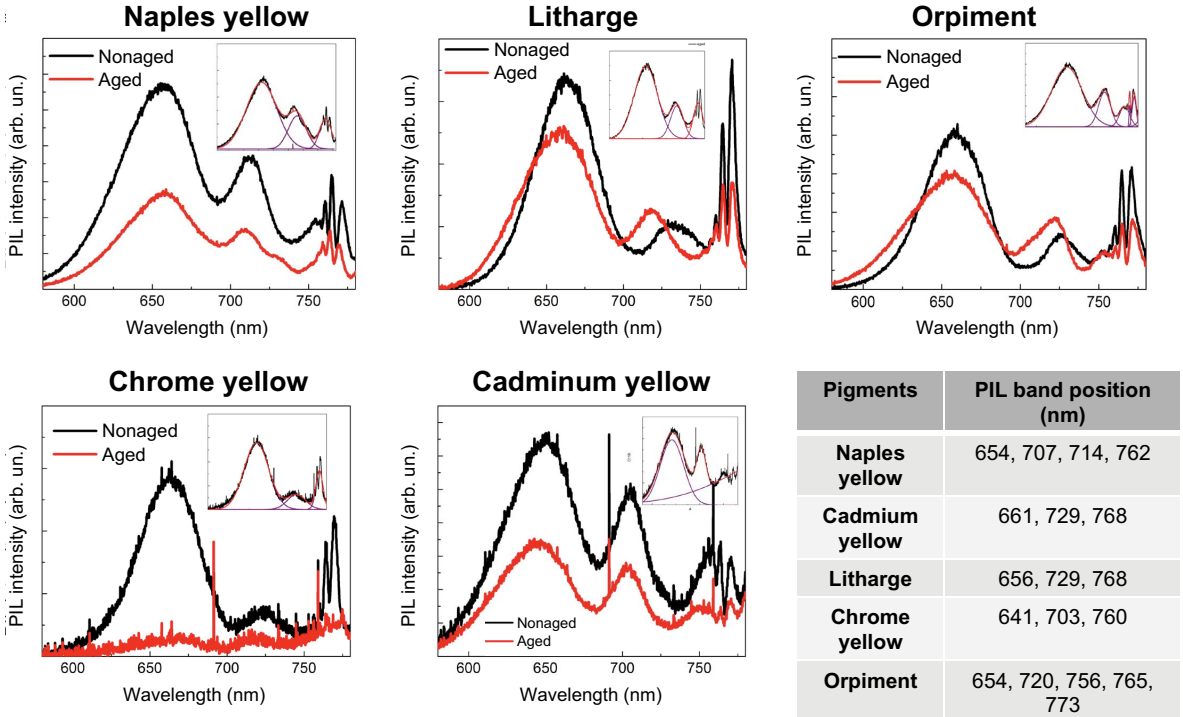

Pigments	PIL band position (nm)
Naples yellow	654, 707, 714, 762
Cadmium yellow	661, 729, 768
Litharge	656, 729, 768
Chrome yellow	641, 703, 760
Orpiment	654, 720, 756, 765, 773

Fig. 2. In-Air-PIL spectra for the different pigments. In-Air-PIL spectra between 580 and 760 nm for all the analyzed elements (as indicated on top of each panel) before aging (black line) and after light irradiation (red line). The insets show the Gaussian analysis on the spectra for identifying the band position and its width. The PIL band positions are listed in the table at the bottom right.

performed on the pigment bulk layer by irradiating the surface with 3-MeV protons (for details regarding the PIXE analysis, refer to the Materials and Method section). Compared to EDX, which provides the surface chemical composition within the first 1 to 2 μm, the PIXE analysis allows determining the elemental chemical composition for deeper depths. For our materials, 3-MeV protons penetrated to depths up to 20 μm (*27*). Representative PIXE data for the Naples yellow, chrome yellow, and orpiment pigments are shown in Fig. 3. All the data indicate that, with enlightening, both the concentration of impurities and trace elements stay constant or decrease. In the case of Naples yellow, e.g., the contribution of Si remains stable at/around approximately 0.65%. S decreases from 2.3 to 1.7%, while the contributions of Fe and Ni decrease from approximately 0.06 and 0.01%, respectively, to below the detection threshold. In addition, the contribution of Ca, likely to be attributed to the canvas or external environmental contamination, decreases from 0.6 to 0.3%. However, there is a marked increase in the concentration of the main component Pb, which increases from 85.2 to 97.3%, partially attributed to the evaporation of elements adsorbed in the pictorial layer such as O and H. Note that, as displayed in Fig. 3, the concentration of Pb decreases with aging. The total number of other elements, detectable and not detectable (our PIXE detector was able to detect elements with atomic weight heavier than that of Na), is reduced with aging. Hence, the total percentage concentration of Pb increases in the aging process. Together, these findings indicate that the light irradiation does not change the chemical composition of the pigment but only reduces the presence of impurities (which can desorb during the light irradiation) and enhances the presence of the major elements. Moreover, the enlightening can change the chemical arrangement of the atoms in the crystalline structure. The analysis of the other pigments, particularly chrome yellow and orpiment, shows very similar results with an unchanged chemical structure before and after aging. Again, in all the pigments, the evaporation of O and H causes an increase in the concentration of the other main elements and impurities.

We performed XRD analysis to shed light onto possible crystalline structure modifications (all details, including graphical figures, can be found in the Supplementary Materials). The XRD patterns of all pigments obtained before aging show a polycrystalline structure composed of the pigment crystalline structure and $CaSO_4$. Again, taking the Naples yellow pigment as a representative example for all pigments, Fig. 4A displays the diffraction pattern for the layers with higher darkening before and after 6 hours of aging. The reflections assigned to the canvas and to the pigment are indicated by the "C" and "P" letters, respectively. The strong $CaSO_4$ presence can be assigned to the canvas, as confirmed by the XRF analysis on the blank canvas illustrated in Fig. 4B. This graph merely indicates the presence of Ca on the white canvas, which is confirmed by the EDX analysis (see the Supplementary Materials). Note that the elements C and S are not detectable using the XRF technique. In the XRD pattern, we do not observe bands that can be attributed to the crystalline nature of the linseed oil. This indicates that the amorphous structure of the binding agent is identical before and after aging and excludes its possible crystallization during the light aging process. The analysis of the XRD patterns of all pigments indicates that, after aging, the $CaSO_4$ line completely disappears or decreases in intensity by at least 90%. This is observed in Fig. 4 and fig. S3 that compare the XRD patterns before (black line) and after (red line) aging. Similarly, all the other bands decrease due to the crystalline nature of the pigments,

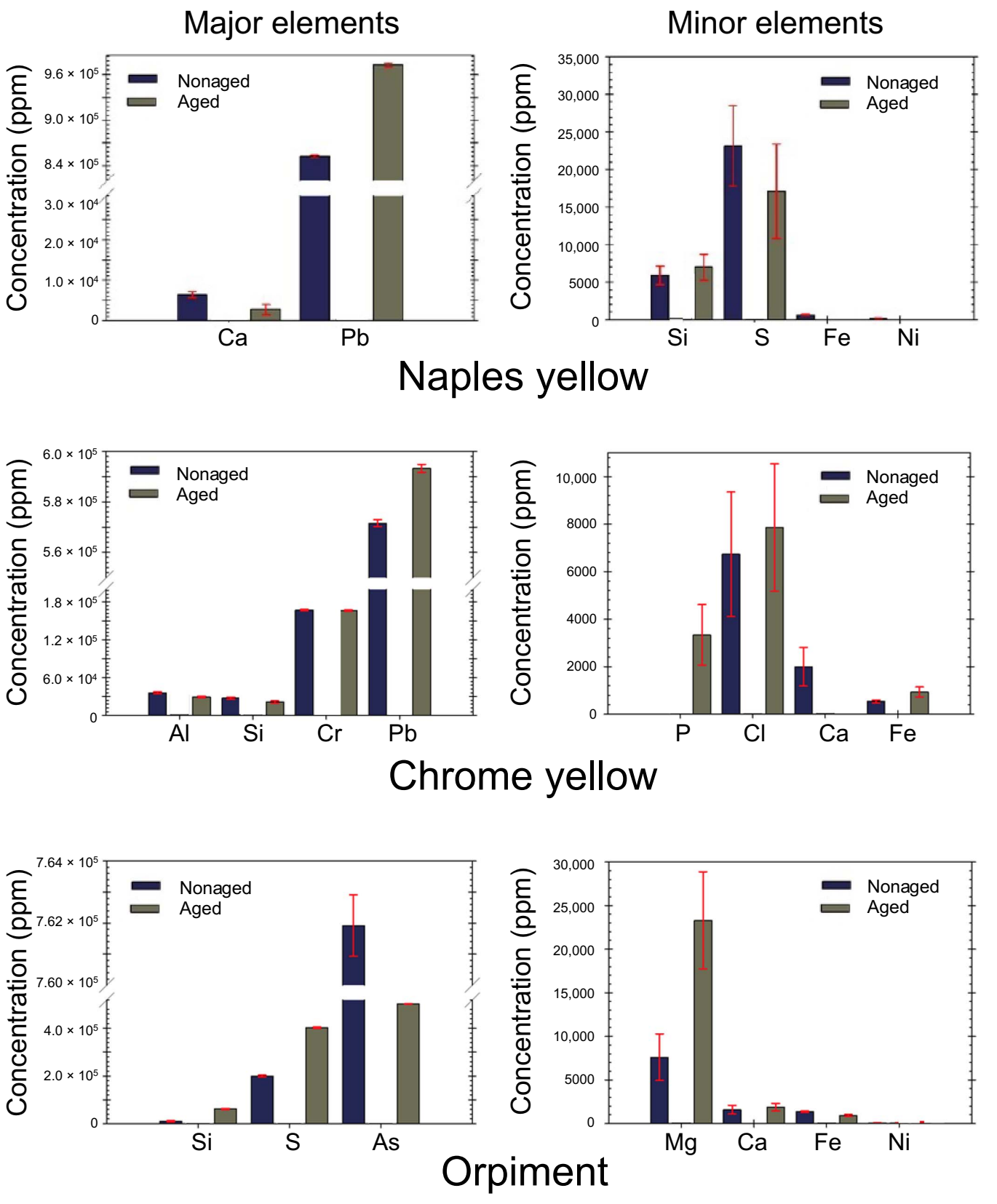

Fig. 3. PIXE results for the different pigments. PIXE results for Naples yellow, chrome yellow, and orpiment (as indicated below the panels); the left panels display the major elements, whereas the right panels display the minor elements. Note that our PIXE diagnostics used a detector only able to detect elements with an atomic mass heavier than Na. The error bars in the concentration measurements performed by the PIXE facility are indicated in red.

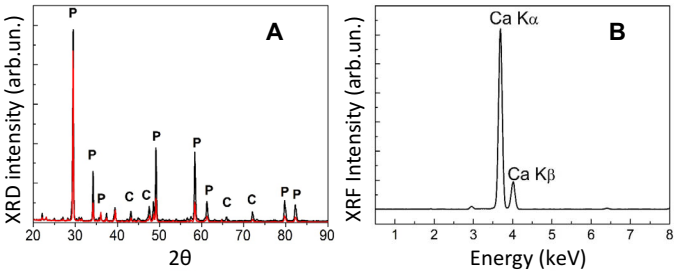

Fig. 4. XRD pattern and XRF spectrum. (**A**) XRD patterns of Naples yellow before (black line) and after (red line) aging, as a representative example for all pictorial layers. The letter P indicates the crystalline lines of the pigments, and C indicates those of the canvas. (**B**) XRF spectrum of the white canvas.

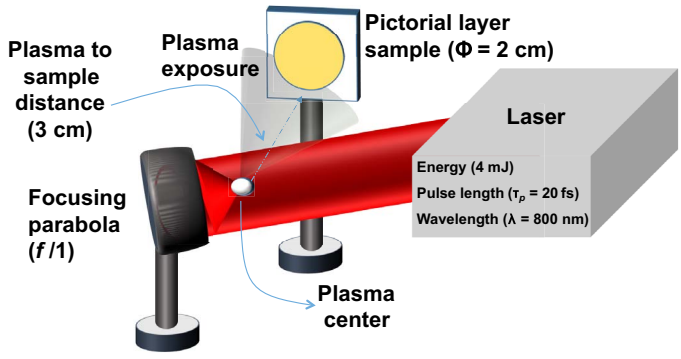

Fig. 5. Experimental setup. Sketch of the experimental setup for the In-Air-PIL.

causing a loss of crystallinity ranging from 30 to 90%. Moreover, we observe a general increase in the crystalline size, which varies from a few Ångstrom to nanometers, indicating a coalescence/aggregation of the pigments' grains, which are too small to be identified in the SEM images but important enough to modify the optical properties of the pigments (XRD results are summarized in the Supplementary Materials). In addition, the crystallographic analysis indicates that, during aging, the crystallinity of the pigments changes from being well-defined to disordered, having identical elemental and molecular composition compared to the original pigment. Similar conclusions can be made for all other pigments (see the XRD tables for all other pigments in the Supplementary Materials).

The decrease in the crystallinity and the increase in the crystal size indicate a general relaxation in the structural lattice, which results in the increase of optical scattering of the pictorial layer and, consequently, in a strong loss of reflectivity. It is well known that when light is irradiated onto nonoriented structures, the light reflectance decreases since a large quantity of light is dispersed in the grain boundary (*28*, *29*, *30*). A direct consequence of the light dispersion is an increase in the absorbance and the bulk scattering, which causes the darkening of the pictorial layer. Moreover, the increase of scattering in the relaxed lattices can easily explain the quenching of the $CaSO_4$ lines after aging. The transmittance through the pictorial layer is strongly reduced, and the x-ray beam does not reach the canvas (the lines that are characteristic of the canvas disappear). We can therefore deduce that the darkening of the yellow pigments under consideration is caused by a strong change in their crystallinity. In addition, we observe an amorphization of the pigments, which lose up to 90 to 95% of their crystallinity. This is confirmed by the saturation of the absorbance curves displayed in Fig. 1. Contrary to other works on yellow pigment darkening (*19*, *20*), we do not observe any formation of oxides or changes in chemical composition within the detection limit of the spectroscopic techniques used [1000 ppm, 0.1 weight % (wt %)]. However, it is likely that the consequence of the lattice deterioration in a real exposure scenario (i.e., including other external environmental agents such as humidity) can favor the interaction of the pigment molecules with O and C adsorbed from the environment or dissolved in the binding agents. As a result, this can lead to the formation of oxalates and carbonates observed, e.g., in other works [see (*9*)].

CONCLUSIONS

In this work, we introduce the use of In-Air-PIL as an alternative to classical chemical and crystallographic techniques used in materials science. We compare the techniques on a series of five yellow pigments, painted as pictorial layers on canvas, to understand the effects of the light aging in atmospheric conditions and at room temperature. The analysis was performed under constant experimental conditions (temperature, humidity, and bacteria presence). We compare morphological, chemical, and crystalline properties of all pigments before and after aging and monitor the optical absorption during the entire light aging process. Our results indicate that the primary effects of the light aging is the darkening of pigments with an increase in optical absorption of about 55% in 120 min for Naples yellow, a pigment with a higher darkening effect. This change in reflectivity is not directly related to chemical or morphological changes, since we do not observe any changes in the chemical composition or in the morphological structure. However, we observe a strong change in the crystallinity of the pictorial layers. The polycrystalline structure of the pigments is reduced by approximately 30 to 90%, while the crystallite size increases by an average value of 35%, indicating a relaxation in the crystal lattice. The structural relaxation causes an increase in the light scattering and absorption into the pictorial bulk and, subsequently, darkening of the layers. In-Air-PIL results, obtained in 5 min, display a luminescence emission having the same bands before and after the light irradiation. This indicates that the chemical composition of the materials remains unaltered; however, changes in their concentration are present. Moreover, a strong variation in the luminescence after irradiation substantiates the transition to a disordered phase. This confirms that the cause of the darkening is strictly related to the changes in the crystal lattice, which favors the effect of other external environmental agents.

MATERIALS AND METHODS

Pictorial layer preparation

We performed our experiments on five pictorial layers composed of two components: (i) the inorganic pigment powder and (ii) linseed oil as binding agent. The enlightening aging behavior of five different yellow pigments (Kremer Pigmente, Germany and Ditta G.Poggi Srl, Via del Gesù, 74/75, 00186 Roma, Italy), i.e., Naples yellow (Kremer pigment no. PY 41.77588), cadmium yellow (Kremer pigment no. PY 35.77205), chrome yellow (Ditta G.Poggi), litharge (Kremer pigment no. PY 46.77577), and orpiment (Kremer pigment no. PY 39.77086), was performed on commercial pigment powder samples (50 mg) mixed with 30 mg of linseed oil. The pictorial solution was subsequently deposited on a commercial canvas holder [mainly composed of calcium sulfate ($CaSO_4 \cdot 2H_2O$)] with dimensions of 2 cm by

2 cm. The drying time for the pictorial layers was fixed to 15 days, while the thickness of the deposited layers was on the order of hundreds of microns. All pigments studied were pure, i.e., without the presence of external impurities caused by the synthesis processes. Chemical analysis conducted on pigment powders (XRF, EDX, and XRD) revealed the absence of impurities within the detection limit of each method (0.1% of weight %).

Light aging

The light aging of pigments was induced by several hours of light exposure at room temperature and in atmospheric conditions, under a white lamp (Scanlite) working in the spectral range between 300 and 800 nm, with a stable power of 3 mW/cm^2 over the entire spectrum. This power corresponds to about 30 times the average irradiation of a 4-m^2 surface (size of a large canvas) in typical exposition conditions; 1 hour of our exposure can be considered equivalent to 1 month of full-time exposure by the commonly used lamps in museums. The lamp power was chosen to prevent the melting of the pictorial layers obtained using the different pigments. The temperature on the canvas was monitored during the entire aging process and was kept stable between 25° and 30°C without reaching temperatures capable of melting the pictorial layers, and that would strongly influence the aging process. A blank canvas and a canvas with a simple deposition of 30 mg of linseed oil also underwent the aging process to investigate their possible influence on the darkening process. All the samples (i.e., the five pictorial layers related to the pigments, the white canvas, and the linseed oil canvas) were submitted simultaneously to the aging process to exclude the influence of experimental and environmental conditions when comparing the aging results. The aging process was stopped after 6 hours of light exposure when all the materials reached a stable saturation value in the optical absorbance. All the aging processes were repeated three times for testing the reproducibility of the results. The optical absorption of the pictorial layers was monitored during the entire aging process at regular time intervals of 15 min. The absorbance reached a saturation value in about 2 hours and remained stable during the successive irradiation. Moreover, we monitored the stability on all pictorial layers for about 4 hours. Our analysis was stopped after 6 hours since additional irradiation times did not affect our measurements.

Optical absorption

Measurements of the optical reflectance during the laser irradiation were obtained, irradiating the pictorial layers with a white lamp (Energetiq LDLS, Laser-Driven Light Source) under confocal microscope conditions (Olympus 900, HORIBA), and the reflected spectra were taken by a TRIAX 320 (HORIBA Jobin Yvon) spectrometer working in the 300 to 800 nm range. The optical absorption was then evaluated using the standard equation

$$a(\lambda) = 1 - \frac{I_r(\lambda)}{I_0(\lambda)} \quad (1)$$

where I_r and I_0 are the reflected and source intensity at each wavelength, respectively. The total optical absorption was evaluated from the integral of $a(\lambda)$ on the whole visible range and normalized to have the maximum value of 1 for a constant value of $a(\lambda) = 1$ in the entire 300- to 800-nm spectral range. We are aware that our formula is simplifying the real physical phenomena, better described by the Kubelka-Munk formula. However, scattering in pigments is most pronounced when the particle diameter is about half that of the light wavelength. In the present case, as the structures have a dimension in the hundreds of nanometers, scattering effects may be neglected.

Analysis using classical morphological and chemical methods

Morphological information on the pictorial layers before and after aging was obtained with SEM microscopy using a Stereoscan SEM microscope working with an energy of 20 keV. Chemical information on all samples was acquired using EDX spectroscopy, under SEM conditions, and realized simultaneously to the image acquisition. The weight % of each element in the pictorial layers was obtained by the standard oxide analysis of the EDX data. The chemical composition of the canvas had been verified by both EDX and XRF. XRF measurements were conducted with an X-123 SDD apparatus (Amptek, USA), equipped with a gold cathode and a beryllium revelator operating at a fixed angle. The PIXE analysis was conducted using the AIFIRA (Applications Interdisciplinaires de Faisceaux d'Ions en Région Aquitaine) accelerator facility of the CENBG (Centre d'Etudes Nucléaires de Bordeaux-Gradignan) located in Bordeaux. The samples were irradiated in air by a proton beam with a nominal energy of 3 MeV, beam current of 500 pA, and beam size with diameter 500 μm for 20 min in He flux. The PIXE spectra were analyzed with a Si(Li) detector Gresham equipped with a "funny filter" (Al foil thickness, 100 μm; hole size, 500 μm) (*31*) to keep the dead time below 10%. Last, the crystallinity of the surfaces was investigated by XRD using a monochromatic Bruker XRD spectrometer working with the Cu Kα line and using a 2Θ configuration at 3° of incident x-ray beam to analyze simply the first nanometers of the target surface. XRD spectra were analyzed using the EVA software distributed by Bruker to determine the crystallinity. A Gaussian model fit was used to evaluate the band centers and full widths at half maximum to obtain the crystallinity size following the well-known Debye-Scherer law.

Analysis using the In-Air-PIL method

The in-air plasma was generated by interaction of a strongly focused-down laser with air (see experimental setup in Fig. 5). We used the Ti:S laser system located at FORTH, which delivered at a 10-Hz repetition rate, 20-fs pulses with carrier wavelength of 800 nm, and an energy of approximately 4 mJ per pulse. This energy corresponds to less than the nominal laser energy (400 mJ) but was chosen to be consistent with the previous In-Air-PIL experimental setup, as described in (*8*), which consisted of a series of transport optics, an on-axis parabola, a series of imaging lines for the plasma analysis, and luminescence collection. The luminescence emission was stimulated by the portion of plasma radiation collected on the sample surface, which was round with a diameter of 2 cm. This size can be reduced with the use of irises or other shielding methods. We performed In-Air-PIL measurements of the pure canvas to evaluate its effect around the pictorial layer. The contribution of the canvas was found to be negligible and was filtered as background from the pure signal. Luminescence emission at an angle of 45° was collected by a lens positioned at 4.5 cm from the irradiated target (focal distance) and transferred through an optical fiber to a spectrometer working in the visible wavelength (VIS) range (OceanOptics USB4000). Each luminescence spectrum was collected with an acquisition time of 500 ms to allow for a sufficient signal-to-noise ratio. For each sample, we collected about 600 spectra to assess the reproducibility of the measurements. Spectra were taken in the dark to eliminate possible sources of background light that would add noise to the measurement.

Given very similar laser parameters to what was used in (*8*), the plasma produced in the interaction between the laser beam and air was similar to the one described in (*8*) and displayed a spheroidal shape with axes of 2 and 3 mm and a photon emission in the visible and near-infrared region with five lines positioned at 1.5, 1.97, 2.12, 2.23, and 2.44 eV. The absence of an ultraviolet line in the plasma excluded the possibility of photoluminescence emission coming from the target sample. The plasma electron current, measured as indicated in (*8*), was about 40 nA in the entire region around the plasma, at a distance of 3 cm from the plasma center, indicating the presence of electrons produced in the plasma and isotropically accelerated.

SUPPLEMENTARY MATERIALS

Supplementary material for this article is available at http://advances.sciencemag.org/cgi/content/full/5/6/eaar6228/DC1

EDX spectra
SEM Images
XRD results
Fig. S1. Summary of EDX spectra for all pigments.
Fig. S2. Summary of SEM image for all pigments.
Fig. S3. Summary of XRD spectra for different pigments.
Table S1. Summary of XRD results for Naples yellow.
Table S2. Summary of XRD results for the cadmium yellow.
Table S3. Summary of XRD results for the litharge.
Table S4. Summary of XRD results for the chrome yellow.
Table S5. Summary of XRD results for the orpiment.

REFERENCES AND NOTES

1. M. Barberio, S. Veltri, F. Stranges, A. Bonanno, F. Xu, P. Antici, AFM and pulsed laser ablation methods for cultural heritage: Application to archeometric analysis of stone artifacts. *Appl. Phys. A* **120**, 909–916 (2015).
2. I. Reiche, E. Chalmin, Synchrotron radiation and cultural heritage: Combined XANES/XRF study at Mn K-edge of blue, grey or black coloured palaeontological and archaeological bone material. *J. Anal. At. Spectrom* **23**, 799–806 (2008).
3. D. Creagh, D. Bradley, Physical Techniques in the Study of Art, Archaeology and Cultural Heritage Vol. 2, Chapter 1 (Elsevier Science 2007).
4. V. Mazel, P. Richardin, ToF-SIMS study of organic materials in cultural heritage: Identification and chemical imaging, in *Organic Mass Spectrometry in Art and Archaeology*, M. P. Colombini, F. Modugno, Eds. (John Wiley & Sons, 2009).
5. M. Dowsett, A. Adriaens, The role of SIMS in cultural heritage studies. *Nucl. Instrum. Methods Phys. Res. B* **226**, 38–52 (2004).
6. S. A. E. Johansson, PIXE: A novel technique for elemental analysis. *Endeavour* **13**, 48–53 (1989).
7. M. Barberio, S. Veltri, M. Scisciò, P. Antici, Laser-accelerated proton beams as diagnostics for cultural heritage. *Sci. Rep.* **7**, 40415 (2017).
8. S. Veltri, M. Barberio, C. Liberatore, M. Scisciò, A. Laramée, L. Palumbo, F. Legaré, P. Antici, Laser stimulated plasma-induced luminescence for on-air material analysis. *Appl. Phys. Lett.* **110**, 021114 (2017).
9. E. Pouyet, M. Cotte, B. Fayard, M. Salomé, F. Meirer, A. Mehta, E. S. Uffelman, A. Hull, F. Vanmeert, J. Kieffer, M. Burghammer, K. Janssens, F. Sette, J. Mass, 2D X-ray and FTIR micro-analysis of the degradation of cadmium yellow pigment in paintings of Henri Matisse. *Appl. Phys. A* **121**, 967–980 (2015).
10. F. Vanmeert, E. Hendriks, G. Van der Snickt, L. Monico, J. Dik, K. Janssens, Back Cover: Chemical mapping by macroscopic X-ray powder diffraction (MA-XRPD) of Van Gogh's *Sunflowers*: Identification of areas with higher degradation risk (Angew. Chem. Int. Ed. 25/2018). *Angew. Chem. Int. Ed.* **57**, 7534 (2018).
11. C. Korenberg, The photo-ageing behaviour of selected watercolour paints under anoxic conditions. *Br. Mus. Tech. Res. Bull.* **2**, 49–57 (2008).
12. S. Aze, J.-M. Vallet, V. Detalle, O. Grauby, A. Baronnet, Chromatic alterations of red lead pigments in artworks: A review. *Phase Transit.* **81**, 145–154 (2008).
13. H. Tan, H. Tian, J. Verbeeck, L. Monico, K. Janssens, G. van Tendell, Nanoscale investigation of the degradation mechanism of a historical chrome yellow paint by quantitative electron energy loss spectroscopy mapping of chromium species. *Angew. Chem. Int. Ed.* **52**, 11360–11363 (2013).
14. D. Goltz, J. McClelland, A. Shellenberg, M. Attas, E. Cloutis, C. Collins, Spectroscopic studies on the darkening of lead white. *Appl. Spectrosc.* **57**, 1393–1368 (2003).
15. S. Hackney, T. Ernst, The applicability of alkaline reserves to painting canvases. *Stud. Conserv.* **39**, 223–227 (2013).
16. J. Kirby, K. Stonor, A. Roy, A. Burnstock, R. Grout, R. White, Seurat's painting practice: Theory, development and technology. *Natl. Gallery Tech. Bull.* **24**, 4–37 (2003).
17. A. Macchia, S. N. Cesaro, L. Campanella, A. Maras, M. Rocchia, G. Roscioli, Which Light for Cultural Heritage: Comparison of Light Sources with Respect to Realgar Photodegradation. *Appl. Spectrosc.* **80**, 637–643 (2013).
18. L. Monico, G. Van der Snicht, K. Janssens, W. De Nolf, C. Miliani, J. Verbeeck, H. Tian, H. Tan, M. Radepont, M. Cotte, Degradation process of lead chromate in paintings by Vincent van Gogh studied by means of synchrotron X-ray spectromicroscopy and related methods. 1. Artificially aged model samples. *Anal. Chem.* **83**, 1214–1223 (2011).
19. L. Monico, K. Janssens, F. Vanmeert, M. Cotte, B. G. Brunetti, G. Van der Snickt, M. Leeuwenstein, J. S. Plisson, M. Menu, C. Miliani, Degradation process of lead chromate in paintings by Vincent van Gogh studied by means of spectromicroscopic methods. Part 5. Effects of nonoriginal surface coatings into the nature and distribution of chromium and sulfur species in chrome yellow paints. *Anal. Chem.* **86**, 10804–10811 (2014).
20. L. Monico, K. Janssens, C. Miliani, G. Van der Snickt, B. G. Brunetti, M. C. Guildi, M. Radepont, M. Cotte, Degradation process of lead chromate in paintings by Vincent van Gogh studied by means of spectromicroscopic methods. 4. Artificial aging of model samples of co-precipitates of lead chromate and lead sulfate. *Anal. Chem.* **85**, 860–867 (2013).
21. C. De Staelen, Rubens's 'Samson and Delilah' in the National Gallery: New facts relating to its provenance. *Burlingt. Mag.* **146**, 467–469 (2004).
22. K. R. Smith-Abbott, "Sons of the Truth, Lovers of Virtue": Painting the Patrician in renaissance Venice. *Vis. Res.* **28**, 43–57 (2012).
23. E. Hendriks, L. Jansen, J. Salvant, E. Ravaud, M. Eveno, M. Menu, I. Fiedler, M. Geldof, L. Megens, M. van Bommel, C. R. Johnson Jr., D. H. Johnson, in *Studying Old Master Paintings: Technology and Practice—The National Gallery Technical Bulletin 30th Anniversary Conference Postprints* (Archetype Publications, 2011), pp. 237–243.
24. The Luminescence Database is a free on-line reference tool for researchers in the fields of cathodoluminescence, photoluminescence, ionoluminescence, and related luminescence spectroscopies; http://www.csiro.au/luminescence/about.html.
25. M. Gaft, R. Reisfed, G. Panczer, *Luminescence Spectroscopy of Minerals and Materials* (Springer, 2005).
26. A. Aliakbari, E. Najafi, M. M. Amini, S. W. Ng, Structure and photoluminescence properties of lead(II) oxide nanoparticles synthesized from a new lead(II) coordination polymer. *Monatsh. Chem.* **145**, 1277–1285 (2014).
27. J. F. Ziegler, M. D. Ziegler, J. P. Biersack, SRIM – The stopping and range of ions in matter (2010). *Nucl. Instrum. Methods Phys. Res. B* **268**, 1818–1823 (2010).
28. H.-C. Weissker, J. Furthmüller, F. Bechstedt, Structural relaxation in Si and Ge nanocrystallites: Influence on the electronic and optical properties. *Phys. Rev. B* **67**, 245304 (2003).
29. J.-H. Lee, K.-H. Ko, B. O. Park, Electrical and optical properties of ZnO transparent conducting films by the sol–gel method. *J. Cryst. Growth* **247**, 119–125 (2003).
30. Y.-S. Kim, W.-P. Tai, S.-J. Shu, Effect of preheating temperature on structural and optical properties of ZnO thin films by sol–gel process. *Thin Solid Films* **491**, 153–160 (2005).
31. S. Gama, M. Volfinger, C. Ramboz, O. Rouer, Accuracy of PIXE analyses using a funny filter. *Nucl. Instrum. Methods Phys. Res. B* **181**, 150–156 (2001).

Acknowledgments: We thank D. Charalambidis and P. Tzallas for their precious support and for providing instrumentation. **Funding:** This work is supported by NSERC Discovery Grant (grant nos. 435416 and RGPIN-2018-05772) and Compute Canada (job: pve-323-ac to P.A.). Concerning the use of the FORTH laser facility, we acknowledge support of this work by the LASERLAB-Europe (grant agreement no. 654148 under the European Union's Horizon 2020 Research and Innovation Programme) and by the project "HELLAS-CH" (MIS 5002735), which is implemented under the "Action for Strengthening Research and Innovation Infrastructures," funded by the Operational Programme "Competitiveness, Entrepreneurship and Innovation" (NSRF 2014-2020) and cofinanced by Greece and the European Union (European Regional Development Fund) and the European Union's Horizon 2020 research and innovation program under Marie Sklodowska-Curie (grant agreement no. 641789 MEDEA). E.S. acknowledges support from the GAICPEU project which has received funding from the Hellenic Foundation for Research and Innovation (HFRI) and the General Secretariat for Research and Technology (GSRT), under grant agreement No [645]. We also acknowledge the support from the ministère des Relations internationales et de la Francophonie du Québec (coopération Québec-Italie, project number 09.103). **Author contributions:** M.B. and P.A. prepared the samples, performed the experiments, and completed the data analysis. E.S. provided support for the laser experiments at

FORTH. S.S. performed the PIXE experimental part and data analysis and interpretation. M.B. and P.A. wrote the paper with the contribution of all authors. M.B. and P.A. conceived and designed the experiment. P.A. coordinated the entire effort. **Competing interests:** The authors declare that they have no competing interests. **Data and materials availability:** All data needed to evaluate the conclusions in the paper are present in the paper and/or the Supplementary Materials. Additional data related to this paper may be requested from the authors.

Submitted 4 December 2017
Accepted 2 May 2019
Published 7 June 2019
10.1126/sciadv.aar6228

Citation: M. Barberio, E. Skantzakis, S. Sorieul, P. Antici, Pigment darkening as case study of In-Air Plasma-Induced Luminescence. *Sci. Adv.* **5**, eaar6228 (2019).